Journal of Thermal Analysis and Calorimetry, Vol. 89 (2007) 2, 547–553

KINETICS OF THERMAL DECOMPOSITION OF MIXED-LIGAND NIKKEL(II) AND COPPER(II) COMPLEXES OF 4-ACYL PYRAZOLONE DERIVATIVE AND PYRIDINE

G.-C. Xu, L. Zhang, L. Liu, G.-F. Liu and D.-Z. Jia[*]

Institute of Applied Chemistry, Xinjiang University, Urumqi 830046, P.R. China

Thermal behaviors of two mixed-ligand complexes, [Ni(PMPP-SAL)$(Py)_3$] and [Cu(PMPP-SAL)Py]·MeOH, (PMPP-SAL= 1-phenyl-3-methyl-4-(salicylidene hydrazide)-propenylidene-pyrazolone-5, Py=pyridine), were studied by TG-DTG-DTA in dynamic air atmosphere. The complexes show the loss of pyridine molecule is followed by the decomposition of the PMPP-SAL anion and give respective metal oxides as residues. Meanwhile, the Ozawa–Flynn–Wall model-free analyses and multivariate non-linear regressions were applied to perform single and overall steps optimization. Kinetic parameters were given and the most probable mechanism functions were suggested in this study.

Keywords: *kinetic studies, mixed-ligand complexes, non-linear regression, thermal analyses*

Introduction

Pyrazolone-5, especially 4-acyl pyrazolones, form an important class of organic compounds and are widely used in biological, analytical applications, catalysis and extraction metallurgy [1–5]. Furthermore, 4-acyl pyrazolone derivatives have a potential to form different types of coordination compounds due to the several electron-rich donor centers [6–9] and tautomeric effect of enol form and keto form [10–12]. Meanwhile, compounds containing hydrazide moieties and their complexes also possess biological activities, especially serving as potential inhibitors for many enzymes [13–15].

During the course of our research, we have synthesized a series of 4-acyl pyrazolone derivatives [16, 17] and reported several transition metal complexes [18–21], but no detailed studies on thermal decomposition and thermal kinetics have been carried out so far. Hence, as a continuation of our earlier study and the interest on the thermal properties of mixed-ligand complexes, we report in this paper the phenomenological, kinetic and mechanistic aspects of thermal decomposition of the nickel(II) and copper(II) complexes of PMPP-SAL and containing pyridine as co-ligand.

Experimental

Materials

Reagents

PMPP (1-phenyl-3-methyl-4-propionyl-5-pyrazolone) and salicylic hydrazide were synthesized according to the references [22, 23]. The ligand PMPP-SAL was synthesized according to the procedure described in the literature [19]. Other chemicals and solvents were analytical grade and commercially available.

Syntheses of the complexes

The synthesis procedure for [Ni(PMPP-SAL)$(Py)_3$] was as follows.

The ligand PMPP-SAL (1 mmol) was dissolved by the addition of an aqueous solution of 1 M NaOH in 15 mL methanol. To which 8 mL of methanol solution of $Ni(OAc)_2·4H_2O$ (1 mmol) and 1.6 mL of a mixture of pyridine and acetonitrile with volume rate 1:1 were added in turn, then the mixture was stirred slightly and loaded into a Teflon-lined stainless steel autoclave, the sealed autoclave was heated to 120°C and kept isothermal for 48 h. After cooled to ambient temperature, the red black crystals were collected by filtered and dried in air. Yield: 0.55 g (83.5% based on nickel).

The [Cu(PMPP-SAL)Py]·MeOH complex was synthesized in a similar way, just using $Cu(OAc)_2·H_2O$ instead of $Ni(OAc)_2·4H_2O$. Yield: 0.42 g (78.2% based on copper).

Methods

Elemental analyses of C, H and N were performed using a PE-2400 analyzer. IR spectra were recorded on a BRUKER EQUINOX-55 spectrophotometer within 400–4000 cm^{-1} with the samples prepared as pellets

* Author for correspondence: jdz@xju.edu.cn

1388–6150/$20.00

Akadémiai Kiadó, Budapest, Hungary
Springer, Dordrecht, The Netherlands

with KBr. The TG-DTA simultaneous measurements were carried out on a Netzsch STA 449C Model instrument. An alumina crucible was used in dynamic air atmosphere (30 cm^3 min^{-1}). The rate of heating was 2, 5 and 10°C min^{-1} and sensitivity of the instruments is 0.1 μg. The crystal structure was determined by a BRUKER SMART 1000 CCD detector and SHELXL-97 crystallographic software package.

Solvothermal syntheses experiments were performed in Teflon-lined stainless steel autoclave with inner volume of 40 mL.

The theoretical base of the kinetics estimation of the thermal decomposition

According to non-isothermal kinetic models, the commonly used kinetic equation of solid thermal decomposition is given as follows:

$$d\alpha/dT=A/\beta\exp(-E_a/RT)f(\alpha) \quad (1)$$

where α is fractional extent of reaction at time t, β the heating rate, E_a the apparent activation energy, $d\alpha/dT$ the rate of the reaction, A the pre-exponential factor, and $f(\alpha)$ is kinetic differential function. Its integral form is as follows:

$$G(\alpha)\int_0^{\alpha} E_a\, d\alpha/f(\alpha)=A/\beta\int_0^{T}\exp(-E_a/RT)dT \quad (2)$$

The fifteen reaction models and mechanism functions [24] were used to fit kinetics curves. The kinetic software from Netzsch was used in this analysis [25–28].

Results and discussion

The elemental analyses results for the ligand and mixed-ligand complexes were listed in Table 1. The results agree well with the given formulae of the compounds. The complexes are stable in air and soluble in most of organic solvents.

Infrared spectra analyses

The main stretching frequencies of the IR spectra of the ligand PMPP-SAL and its mixed-ligand complexes are tabulated in Table 2. The ligand spectrum shows a medium intensity band at around 3249 cm^{-1}, assigned to the hydrogen bond NH and OH stretching vibrations. The strong bands at 1663 and 1614 cm^{-1} are respectively allocated as $\nu_{C=O}$ of the hydrazide and $\nu_{C=O}$ of pyrazolone-ring. From above analysis, it is concluded that the ligand is mainly existed in keto-form in the solid-state. However, in the spectra of the complexes, the C=O bands are both absent. Meanwhile, a new band is observed around 1440 cm^{-1} due to ν_{C-O^-}, the band at around 510 cm^{-1} is assigned to ν_{M-O}. All of these demonstrate that the oxygen atoms of carbonyl have formed coordinate bonds with the metal ion. From these observations, it is concluded that the ligand reacts in the enol form when coordinated to the metal ions in the solvent and the two enolic protons are replaced by M(II) in the complexes. The results also confirmed by the crystal structure analyses.

In the complexes spectra, the NH stretching vibration disappears and two new bands at about 1600 and 1576 cm^{-1} appear, they are respectively allocated as $\nu_{-C=N-N=C-}$ of hydrazone and the coordinated pyridine nitrogen. All of these demonstrate that the nitrogen atom of imino-group of hydrazone is coordinated to M(II). The new bands at about 460 cm^{-1} for the complexes are assigned to ν_{M-N}. It further confirms that the nitrogen atom of the imino-group bonds to the transition metal ion.

In the ligand spectrum, the strong band observed at 1308 cm^{-1} is assigned to ν_{C-OH} stretching vibration of phenolic oxygen. This band shifts very feeble in the spectra of metal complexes, indicating the non-coordination of the phenolic oxygen atom to the central metal ion.

Thermal decomposition

[Ni(PMPP-SAL)$(Py)_3$]

The simultaneous TG-DTG-DTA curves of the [Ni(PMPP-SAL)$(Py)_3$] are preserved in Fig. 1. The decomposition of the mixed-ligand complex undergoes in three stages. The endothermic degradation of two mole pyridine molecules takes place in the first stage between 90 and 160°C with a mass loss of 23.96% (calcd.: 24.02%). The maximum rate of mass loss is indicated by the DTG peak at 142°C. The residue at the first stage was found to be [Ni(PMPP-SAL)(Py)]. The

Table 1 The elemental analyses for the mixed-ligand complexes

Compound	Formula mass/g mol^{-1}	Found (calcd.)/%		
		C	H	N
PMPP-SAL	364.40	65.44 (65.92)	5.81 (5.53)	15.28 (15.37)
[Ni(PMPP-SAL)$(Py)_3$]	658.39	63.94 (63.85)	5.13 (5.05)	14.78 (14.89)
[Cu(PMPP-SAL)Py]·MeOH	537.07	58.32 (58.15)	5.07 (5.07)	13.21 (13.04)

Table 2 IR bands assignment for ligand and the complexes/cm^{-1}

Compound	ν_{O-H}	ν_{N-H}	$\nu_{C=O}$	ν_{C-O^-}	$\nu_{C=N}$	$\nu_{C=N_{Py}}$	ν_{C-OH}	ν_{M-O}	ν_{M-N}
PMPP-SAL	3249	3249	1663, 1614	–	–		1308	–	–
[Ni(PMPP-SAL)(Py)$_3$]	3176	–	–	1445	1599	1576	1305	506	457
[Cu(PMPP-SAL)Py]·MeOH	3313	–	–	1453	1602	1576	1301	511	464

second stage between 160 and 210°C corresponds to decomposition of the remaining pyridine molecule and one endotherm is observed in the DTA trace. The observed mass loss is 11.81% which is consistent with the theoretical value of 12.01%. With heating, the decomposition of the ligand PMPP-SAL was followed. The third stage, which occurs in the temperature range 340–420°C with DTG peak at 388, 402°C, corresponds to the decomposition of the ligand, the observed mass loss (52.12%) is roughly coincide with the calculated value (52.20%). This step appears in the DTA curve as a broad exotherm with T_{max}=402°C and ΔH=12.9 kJ g^{-1}. The final residue, estimated as nickel oxide, has the observed mass 12.53% as against the calculated value of 11.34%.

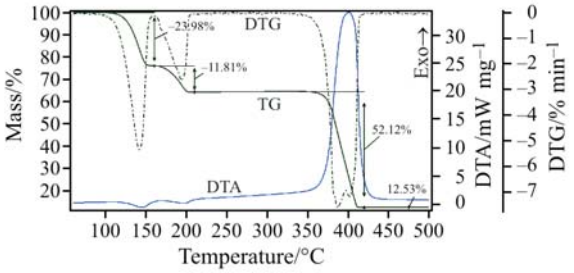

Fig. 1 The TG-DTG-DTA curves of [Ni(PMPP-SAL)(Py)$_3$], heating rate: 5°C min^{-1}

The decomposition procedure of [Ni(PMPP-SAL)(Py)$_3$] can also be demonstrated by the crystal structure of the complex (Fig. 2). With regard to the bond distances, the Ni–N(pyridine) (Ni–N5, Ni–N6 and Ni–N7) distances are longer than other coordinating bond lengths (Table 3). In theory, these bonds are less stable and easy to be broken down. Therefore, the pyridine molecules were considered to be expelled before the decomposition of the PMPP-SAL anion. Among the three pyridine molecules, Ni–N5 and Ni–N7 bond lengths (2.132(3), 2.148(3) Å) are longer than Ni–N6 bond length (2.082(3) Å), indicating that the bond strengths of pyridyl nitrogen atom coordinated to Ni(II) are different and Ni–N6 is stronger than Ni–N5 and Ni–N7. Thus, Ni–N6 bond was considered to be broken down following Ni–N5 and Ni–N7 bonds. The TG curve shows that two pyridine molecules were lost first and the removal of the remaining pyridine molecule was followed.

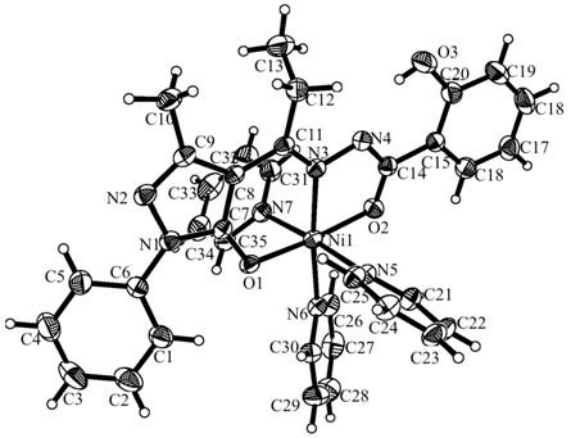

Fig. 2 The molecular structure of [Ni(PMPP-SAL)(Py)$_3$] with thermal ellipsoids shown at 30%

Table 3 Partial bond distances of [Ni(PMPP-SAL)(Py)$_3$]

Bond	Bond distance/Å	Bond	Bond distance/Å
Ni1–O1	2.006(3)	Ni1–O2	2.034(3)
Ni1–N3	1.996(3)	Ni1–N6	2.082(3)
Ni1–N5	2.132(3)	Ni1–N7	2.148(3)

Therefore, the thermal decomposition process of [Ni(PMPP-SAL)(Py)$_3$] complex can be expressed by the following scheme:

$$[Ni(PMPP\text{-}SAL)(Py)_3] \rightarrow [Ni(PMPP\text{-}SAL)Py] \rightarrow [Ni(PMPP\text{-}SAL)] \rightarrow NiO$$

[Cu(PMPP-SAL)Py]·MeOH

The thermal model of [Cu(PMPP-SAL)Py]·MeOH is shown in Fig. 3 and it indicated that the thermal decomposition takes place in three distinct stages. In the first stage between 80 to 115°C, the noncoordinated crystal methanol molecule moves as shown as one maxima in the DTG curve at 107°C with a 4.63% mass loss (calcd.: 5.96%). The second stage starts at 145 and end at 212°C, the corresponding mass loss (14.51%) is due to the degradation of one mole pyridine molecule which is in agreement with the calculated value (14.73%). DTA curve shows two endotherms at 108 and 199°C for the above two stages. The third stage, which occurs in the temperature range 315–405°C, corresponds to the decomposition

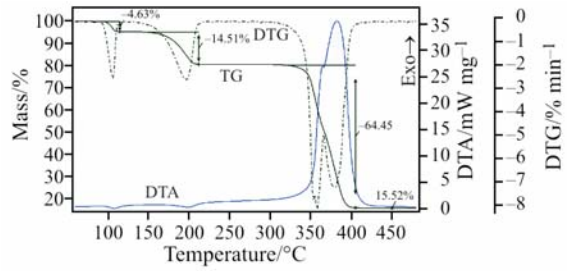

Fig. 3 The TG-DTG-DTA curves of [Cu(PMPP-SAL)Py]·MeOH, heating rate: 5°C min^{-1}

of the ligand PMPP-SAL, and the observed mass loss (64.45%) coincides with the theoretical value (64.50%). The DTA shows a large exothermic peak at 383°C corresponding to this stage. Mass constancy is attained at around 420°C. The end product, estimated as CuO, has the observed mass of 15.52% compared with the calculated value of 14.81%.

Kinetic analyses

The apparent activation energy of the decomposition process in non-isothermal conditions can be calculated by model-free isoconversional method [29–35]. The model-free kinetic analyses have the advantage of alleviating the need to select a specific kinetic model and hence any dependence on this choice. The Netzsch thermokinetics software package has the capacity to perform model-free kinetic analyses. According to our experience the significance of the model-free analyses lies in its function as preliminary stage of non-linear regression. The determination of kinetic parameters by means of the non-linear regression is an iterative process. The preset of start values for the parameters is necessary. Here the model-free estimation of the activation energy means a great help for the non-linear regression for being able to deliver start values. Furthermore the multi-step feature of a process often can only be detected from the dependence of the activation energy on the reaction degree [36].

In this study, the Ozawa–Flynn–Wall model-free analysis and multivariate non-linear regression were applied to perform single and overall steps optimization. Kinetic parameters were given and the most probable mechanism functions were suggested (Table 4).

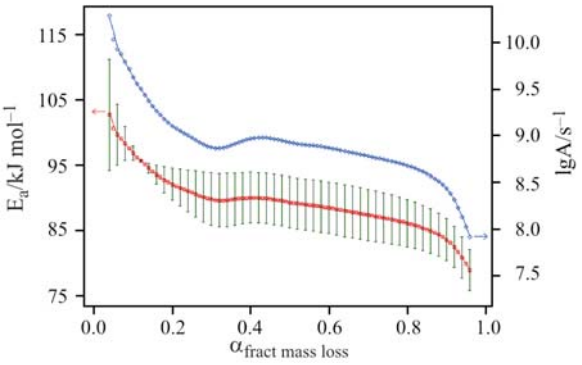

Fig. 4 A plot of E_a and log$A$ as a function of α for the first stage of [Ni(PMPP-SAL)(Py)$_3$] based on the OFW model-free method using TG results. The error limits specified by bars

Kinetic TG analysis of [Ni(PMPP-SAL)(Py)$_3$]

The TG data for the three decomposition stages of this complex were analyzed by model-free method and non-linear fit to 15 mechanism functions.

Figure 4 shows that the activation energy E_a of the first stage is nearly independent of the extension of conversion α. Ozawa–Flynn–Wall model-free analysis reveals that the average activation energy value is about 89 kJ mol^{-1}. This indicates that the first decomposition stage is a single-step reaction, so single-step reaction mechanism was selected. Considering fitting quality (characterized by correlation coefficient and relative precision), the C1 B model is the most suitable one for this reaction. The kinetic parameters and statistical characterization after the multivariate non-linear regression are listed in Table 4 and graphic presentation of the curve fitting are shown in Fig. 5. It can be seen that the experimental data and the non-linear regression model fit well.

The Ozawa–Flynn–Wall model-free analysis shows that the average activation energy value of the second stage varies little with the mass loss, and the activation energy value is about 95 kJ mol^{-1}. This indicates that this stage is also a single-step reaction. The fitted curves are showed in Fig. 6.

It is clear in Fig. 7 that the activation energy of the third stage assumes a value of 137 kJ mol^{-1} at the beginning and, with increasing mass loss, it drops

Table 4 The optimized mechanism functions and kinetic parameters of two mixed-ligand complexes

Complex	Stage	Mechanism	E_a/kJ mol^{-1}	lg$A$/s^{-1}	Reaction order n	Exponent α	Correction coefficient
[Ni(PMPP-SAL)(Py)$_3$]	I	C1 B	89.1836	8.5676	1.0000	0.7703	0.99941
	II	Bna	112.5905	10.2767	3.6685		0.99935
	III	Fn	176.7993	11.9930	3.1691		0.99935
		Fn	154.1651	12.1090	7.5229		
[Cu(PMPP-SAL)Py]·MeOH	I	Fn	361.5583	48.9240	0.7256		0.99957
		Fn	240.1268	31.3189	0.5876		
	II	Bna	128.3496	12.0453	1.1462	7.1947E-2	0.99894

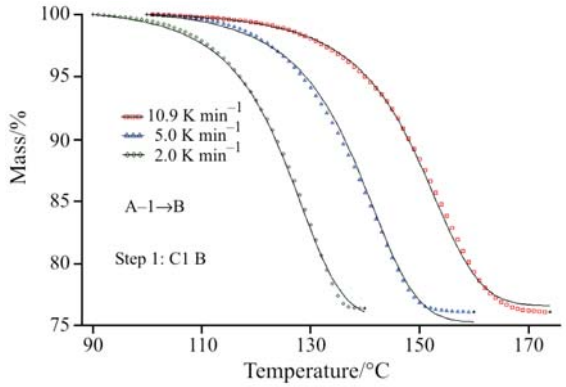

Fig. 5 Fit of the first stage of the TG curve of [Ni(PMPP-SAL)(Py)$_3$], simulated with reaction type C1 B; signs – measured, — – calculated

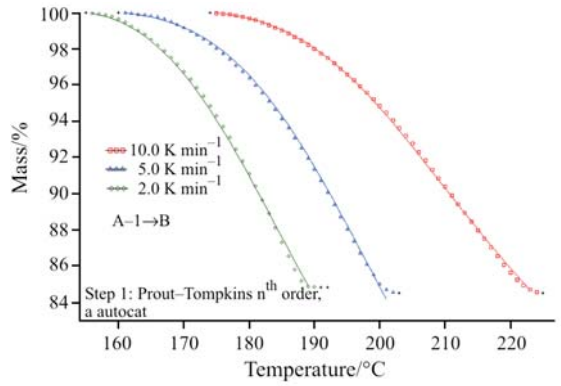

Fig. 6 Fit of the second stage of the TG curve of [Ni(PMPP-SAL)(Py)$_3$]; signs – measured, — – calculated

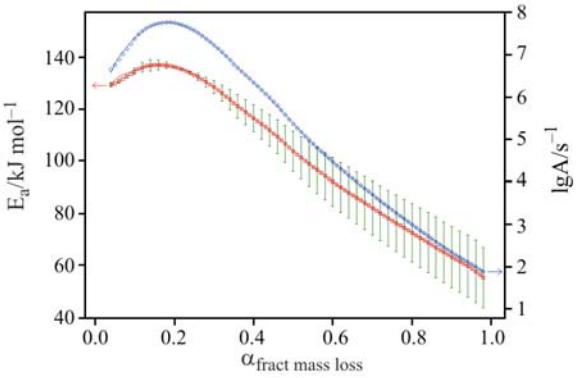

Fig. 7 A plot of E_a and log$A$ as a function of α for the third stage of [Ni(PMPP-SAL)(Py)$_3$] based on the OFW model-free method using TG results. The error limits specified by bars

slowly to a value of 57 kJ mol^{-1}. This dependence of the activation energy E_a on α (fractional mass loss) is an indication that the overall reaction contains two steps. Hence two-step mechanism model was used to fit it. In this work Fn–Fn model is determined as the most-probable model. The calculated curves were fitted to the experimental ones (Fig. 8).

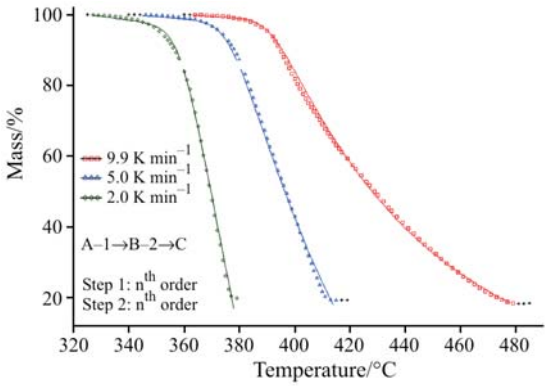

Fig. 8 Fit of the third stage of the TG curve of [Ni(PMPP-SAL)(Py)$_3$]; signs – measured, — – calculated

In conclusion, the thermal decomposition of complex [Ni(PMPP-SAL)(Py)$_3$] occurs in three stages. The Ozawa–Flynn–Wall model-free analysis and multivariate non-linear regression method are used to the overall decomposition process. The best fitted models and kinetic parameters were determined. The first stage adopts the single-step reaction model, and the reaction mechanism is C1 B, relevant E_a is 89.1836 kJ mol^{-1}. The value agrees well with that from OFW analysis. The second stage also adopts A→B single-step reaction model and the reaction mechanism function is Bna. The third stage adopts the A→B→C reaction model and the mechanism function is Fn–Fn.

Kinetic TG analysis of [Cu(PMPP-SAL)Py]·MeOH

The stages of the removal of methanol molecule and pyridine molecule were analyzed by the multivariate non-linear regression analyses. The start values for the parameters were taken from the OFW model-free analyses. The 15 reaction mechanism functions were tested to fit the curves.

According to the Ozawa–Flynn–Wall model-free analysis result, the activation energy for the first stage assumes a value of 310 kJ mol^{-1} at the beginning and at the end it drops to a value of 256 kJ mol^{-1}. The E_a decreases with extent of conversion α indicates that the decomposition reaction contains at least two steps. So a two-step consecutive reaction A→B→C was selected. Multivariate non-linear-regression method shows Fn–Fn model is the best fit model with highest correlation coefficient. Figure 9 shows the experimental data and the non-linear regression model fit well. The calculated apparent activation energies are consistent with Ozawa–Flynn–Wall model-free analysis.

Figure 10 shows that the activation energy and pre-exponential factor of the second stage are independent of the extension of conversion, the activation energy value is about 110 kJ mol^{-1}. This clearly indicates that the second stage is a single-step reaction. So

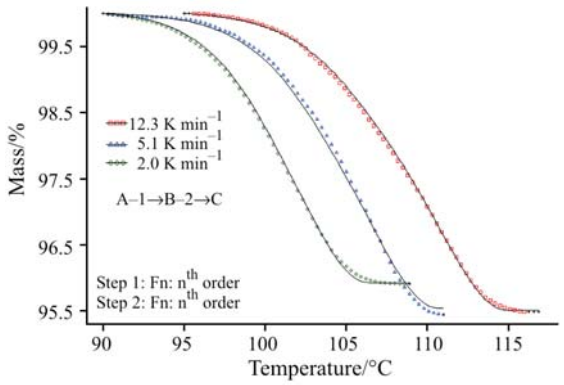

Fig. 9 Fit of the first stage of the TG curve of [Cu(PMPP-SAL)Py]·MeOH; signs – measured, — – calculated

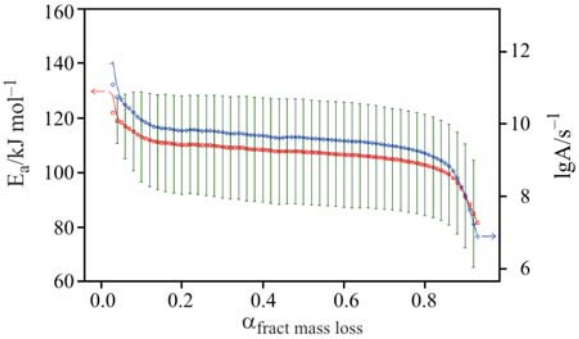

Fig. 10 Dependence of E_a and log$A$ *vs.* α for the second stage of [Cu(PMPP-SAL)Py]·MeOH based on the OFW method

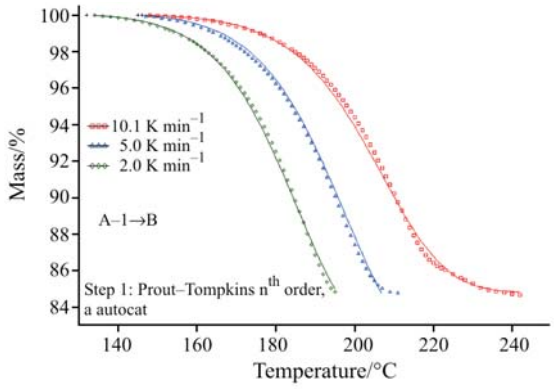

Fig. 11 The second stage of the [Cu(PMPP-SAL)Py]·MeOH decomposition was the best fit to mechanism function; signs – measured, — – calculated

single reaction mechanism was used to fit, the results were satisfied (Fig. 11).

In conclusion, the thermal decomposition of complex [Cu(PMPP-SAL)Py]·MeOH was studied in air using TG-DTG-DTA analyses. TG-DTA curves show that the decomposition occurs in three stages. The most-probable kinetic models of the first and second stages have been estimated with multivariate nonlinear regression method. The optimized mechanism function of first stage is A→B→C sequential reaction model, the mechanism function is Fn–Fn, relevant E_a are 361.5583, 240.1268 kJ mol^{-1}, and log$A$ are 48.9240 and 31.3189 s^{-1}. The calculated apparent activation energies of the fitted model are consistent with those calculated by isoconversional method using original data. The second stage adopts single-step reaction model and the reaction mechanism function is Bna. We tried to use single-step and multi-step mechanism model to fit the third stage of decomposition reaction, unfortunately, a high quality of fit has not achieved.

Acknowledgements

This work was supported by the National Natural Science Foundation of China (No. 20366005 and 20462007) and Scientific Research Foundation in Xinjiang Educational Institutions (XJEDU2005S01).

References

1 N. Raman, A. Kulandaisamy, A. Shunmugasundaram and K. Jeyasubramanian, Transit. Met. Chem., 26 (2001) 131.
2 T. Yoshikuni, J. Mol. Catal. A-Chem., 148 (1999) 285.
3 B. A. Uzoukwu, P. U. Adiukwu, S. S. Al-Juaid, P. B. Hitchcock and J. D. Smith, Inorg. Chim. Acta, 250 (1996) 173.
4 Z. Y. Yang, R. D. Yang, F. S. Li and K. B. Yu, Polyhedron, 19 (2000) 2599.
5 W. F. Yang, S. G. Yuan, Y. B. Xu, Y. H. Xiao and K. M. Fang, J. Radioanal. Nucl. Ch., 256 (2003) 149.
6 A. K. El-Sawaf and D. X. West, Transition Met. Chem., 23 (1998) 417.
7 N. Kalarani, S. Sangeetha, P. Kamalakannan and D. Venkappayya, Russ. J. Coord. Chem., 29 (2003) 845.
8 C. Pettinari, F. Marchetti, C. Santini, R. Pettinari, A. Drozdov, S. Troyanov, G. A. Attiston and R. Gerbasi, Inorg. Chim. Acta, 315 (2001) 88.
9 F. Marchetti, C. Rettinar, R. Pettinari, A. Cingolani, D. Leonesi and A. Lorenzotti, Polyhedron, 18 (1999) 3041.
10 O. N. Kataeva, A. T. Gubaidullin, I. A. Litvinov, O. A. Lodochnikova, L. R. Islamov, A. I. Movchan and G. A. Chmutova, J. Mol. Stuct., 610 (2002) 175.
11 Y. Akama and A. Tong, Microchem. J., 53 (1996) 34.
12 Y. Akama, A. Tong, N. Matsumoto, T. Ikeda and S. Tunaka, Vib. Spectrosc., 13 (1996) 113.
13 M. F. Iskander, L. Sayed, A. F. M. Hefny and S. E. Zayan, J. Inorg. Nucl. Chem., 38 (1976) 2209.
14 G. H. Havanur and V. B. Mahale, Indian J. Chem., 26A (1987) 1063.
15 H. Adams, D. E. Fenton, G. Minardi, E. Mura and M. Angelo, Inorg. Chem. Commun., 3 (2000) 4.
16 X. C. Tang, D. Z. Jia, K. B. Yu, X. G. Zhang, X. Xia and Z. Y. Zhou, J. Photochem. Photobiol. A: Chem., 134 (2000) 23.

17 L. Liu, D. Z. Jia, Y. L. Ji and K. B. Yu, J. Photochem. Photobiol. A: Chem., 154 (2003) 117.
18 L. Liu, D. Z. Jia and Y. L. Ji, Synth. React. Inorg. Met.-Org. Chem., 32 (2002) 739.
19 Y. L. Ji, L. Liu, D. Z. Jia and K. B. Yu, Chinese J. Inorg. Chem., 19 (2003) 345.
20 L. Zhang, L. Liu, D. Z. Jia and K. B. Yu, Struct. Chem., 15 (2004) 327.
21 L. Zhang, L. Liu, D. Z. Jia, G. C. Xu and K. B. Yu, Inorg. Chem. Commun., 7 (2004) 1306.
22 B. S. Jensen, Acta Chem. Scand., 13 (1959) 1668.
23 R. Q. Huang, H. L. Wang and J. Zhou, Preparation of Organic Intermediates, Chemistry Industrial Press, China 1997, p. 109.
24 D. Dollimore, P. Tong and K. S. Alexander, Thermochim. Acta, 282–283 (1996) 13.
25 J. Opfermann, J. Therm. Anal. Cal., 60 (2000) 641.
26 V. Logvinenko, A. Minina, Y. Mikhaylov, Y. Yukhin and B. Bokhonov, J. Therm. Anal. Cal., 74 (2003) 407.
27 J. H. Hong, T. Y. Yi, J. Min, C. J. Cong and K. L. Zhang, Thermochim. Acta, 440 (2006) 31.
28 S. K. Padhi, Thermochim. Acta, 448 (2006) 1.
29 H. L. Friddman, J. Polym. Sci., 6 (1965) 183.
30 T. Ozawa, Bull. Chem. Soc. Jpn., 38 (1965) 1881.
31 K. Uemura, S. Kitagawa, K. Saito, K. Fukui and K. Matsumoto, J. Therm. Anal. Cal., 81 (2005) 529.
32 V. Alvarez, E. Rodriguez and A. Vazquez, J. Therm. Anal. Cal., 85 (2006) 383.
33 L. S. Guinesi, C. A. Ribeiro, M. S. Crespi, A. F. Santos and M. V. Capela, J. Therm. Anal. Cal., 85 (2006) 301.
34 S. Vyazovkin, Thermochim. Acta, 355 (2000) 155.
35 P. Šimon, J. Therm. Anal. Cal., 76 (2004) 123.
36 J. R. Opfermann, E. Kaisersberger and H. J. Flammersheim, Thermochim. Acta, 391 (2002) 119.

Received: February 16, 2005
Accepted: January 31, 2007

DOI: 10.1007/s10973-005-6947-6